A Rotor Tip Vortex Tracing Algorithm for Image Post-Processing

Austin D. Overmeyer
Aerospace Engineer
U.S. Army Aviation Development Directorate (ADD)
AeroFlightDynamics Directorate (AFDD)
Hampton, VA, 23681

ABSTRACT

A neurite tracing algorithm, originally developed for medical image processsesing, was used to trace the location of the rotor tip vortex in density gradient flow visualization images. The tracing algorithm was applied to several representative test images to form case studies. The accuracy of the tracing alogrithm was compared to two current methods including a manual point and click method and a cross-correlation template method. It is shown that the neurite tracing alogrithm can reduce the post-processing time to trace the vortex by a factor of 10 to 15 without compromising the accuacy of the tip vortex location compared to other methods presented in literature.

INTRODUCTION

The rotor tip vortex is a key factor in the aerodynamics, aeromechanics and noise of a helicopter. The flow field induced by the tip vortex has an important role in the aerodynamic performance of the rotor. The tip vortex interaction with the fuselage can lead to reduced fatigue life of structural components and poor aerodynamic performance of control surfaces. Blade vortex interaction (BVI) is a large source of noise for the vehicle. Improvements in these areas require advancements in computational modeling and methods, which in turn relies upon accurately measuring the tip vortex properties. Qualitative optical flow field measurements such as Particle Image Velocimetry (PIV) and Laser Doppler Velocimetry (LDV) require a priori knowledge of the vortex location to acquire detailed flow field measurements. Experimental setups for these measurement techniques can be aided by using density gradient flow visualization techniques to locate the vortex.

Flow visualization of the rotor tip vortex has been utilized since the 1950s using balsa wood dust to visualize the rotor wake, Ref. 1. More popular, density gradient methods such as shadowgraph, schlieren and more recently background oriented schlieren (BOS) have also been used. Conventional schlieren and BOS are sensitive to the first derivative of the density variation while shadowgraph is a second derivative representation of the density field. Early density gradient efforts focused on qualitative visualization of the tip vortex using a single camera setup. These single camera setups were extended to determine the radial and axial extent of the tip vortex by making planar optical assumptions. Numerical predictions of the tip vortex location are generally compared to the measured tip vortex location in terms of axial and radial extent of the vortex rather than the 3-D location of the vortex. The aperiodic and complex path of the tip vortex in both forward flight and hover in ground effect (IGE) limits the ability of single camera systems to experimentally measure the tip vortex location in 3-D space. An improvement in the measurement technique could aid in the development to prediction tools.

Recently, multi-camera systems have been used to measure the tip vortex location in 3-D space using photogrammetric methods, Refs. 2–4. These multi-camera systems have had a high degree of success in measuring the tip vortex location in 3-D space in both flight and wind tunnel testing. Multi-camera photogrammetry measurements require the tip vortex location in each image be assigned a pixel location. The pixel location in all of the images can be used to determine the 3-D position of the vortex by using the fundamentals of photogrammetry. This more complex measurement technique requires additional post-processing time, which limits the ability of the researcher to process large volumes of data. Previous researchers have automated many of the post-processing subroutines such as camera calibration, bundle adjustments, and object space coordinate calculations. The bottleneck of the current post-processing schemes is in determining the pixel location of the vortex filament.

Regardless of the imaging technique used to visualize the tip vortex or testing method (flight or wind tunnel), the pixel position of the vortex must be determined to calculate the vortex location in space. The data processing steps are clearly explained by Schairer et. al. in Section V. of Ref. 2. Step three from Section V. requires the vortex filaments position to be determined for each image. In most cases, the pixel position was determined by manual point-click selection.

An alternative method is a cross-correlation template method previously developed for fixed-wing applications as described by Ref. 5. In fixed-wing applications, the vortex

diffuses naturally in the streamlines of the flow as the vortex convects downstream from the wing. The cross-correlation template method relies on the researcher to select the start of the vortex to use as a template of the vortex signature. The vortex signature template is then marched column by column, for a nearly horizontal vortex, or row by row, for a nearly vertical vortex, across the image with the vortex location being defined as the pixel location where the cross-correlation to the template is a maximum. The template is updated every column/row to account for growth of the vortex. This method works extremely well for nearly horizontal or vertical vortices with high signal to noise ratios (SNR) and without background non-uniformities.

Non-uniformities in the background and flow features alike can create difficulties in tracing the tip vortex. In wind tunnel environments, retro-reflective backgrounds are typically used to increase the amount of light return to the camera sensor. Even in controlled wind tunnel environments the retro-reflective backgrounds are extremely sensitive to dirt, oil and installation handling that cause small dark blemishes in the image. In large wind tunnels, several background panels are required, in turn creating seams in the background which appears as dark lines in the images. For BOS images both in wind tunnel and flight test, similar issues of non-uniformity in the background are typically encountered. If a vortex path is projected onto a noisy background area, the SNR is significantly reduced. In addition to non-uniform backgrounds, several flow features of the tip vortex make it difficult to track its path. In hover the rotor tip vortex is convected downward in a helical path. In a 2-D image the helical path is projected onto the camera sensor by a combination of a horizontal and vertical lines. The more complex path of a rotor tip vortex requires a higher order tracing algorithm than that of the cross-correlation template method. For cases where the density gradient of the tip vortex is small, e.g., low thrust cases, the image contrast between the vortex and background is small, creating a low SNR.

An ideal tracing technique should be able to reliably trace complex vortex paths with minimal user interaction while being insensitive to background noise. The objective of this paper is to present a semi-automatic vortex tracing algorithm to aid in the post-processing of density gradient tip vortex flow visualization images. The tracing algorithm will be compared to the cross-correlation template method and manual traces.

TRACING ALGORITHM

To achieve the goal of an improved rotor tip vortex tracing technique, medical imaging tracing tools were explored. The field of medical imaging has devoted a large portion of research into tracing the human nervous system. An image of the human nervous system is in many ways similar to that of a density gradient image of a rotor tip vortex. A fluorescence microscopy image of the human brain from Ref. 6 is compared to a shadowgraph image of a tip vortex from a hovering rotor IGE in Fig. 1. The neuron image is comprised of bright elongated structures on a noisy background, where

the shadowgraph image is comprised of dark elongated structures on noisy background. For BOS images, the pixel shift is calculated using a cross-correlation algorithm with a reference wind-off image. The pixel shift is a function of the first derivative of the density field. By taking the derivative in the same direction as the pixel shift calculation, a virtual shadowgraph image is produced. The derivative reduces the sensitivity of the BOS image but it is required for the proposed tracing algorithm. As it will be shown in the Results section, the first derivative removes the abilities to distinguish the flow turbulence around the tip vortex but not the ability to trace the vortex.

Neurite Tracer

Based on the similarities of these types of images, neurite tracing algorithms were proposed to be used to trace the tip vortex in individual images. The neurite tracing algorithm calculates the "neuriteness" or in this case the "vortexness" of every pixel in the image. This is computed by convolution with the second-order derivatives of the Gaussian kernel. An eigenvalue analysis of the Hessian matrix assigns each pixel a value based on the likehood that it is a vortex. By using a second-order technique, background intensity discontinuities are suppressed since they are first-order structures. The algorithm is considered semi-automatic because it requires the user to select a start and end point of the vortex. The path between the two points is calculated by computing a cost function for each pixel to any eight of the neighboring pixels. The shortest path of the cost function is computed using a Dijkstra shortest-path algorithm. The details of the algorithm are contained in Appendix of Ref. 6 and were not altered for this work. The NeuronJ plugin from Ref. 6 for ImageJ, Ref. 7, was used throughout this work.

NeuronJ Parameters

The NueronJ plugin requires 5 user specified input parameters. The parameters and a brief description of each are shown in Table 1. In order to determine the effect of these parameters on vortex traceability, a parametric study was conducted. A similar study was conducted by Meijering et al. in Ref. 6 during validation of the algorithm. The Gaussian smoothing scale (σ) can be used to help suppress background noise for a given vortex width. For this study, a range of values from one to four were considered. The Gaussian smoothing scale is proportional to SNR ratio and in cases of high SNR a value of $\sigma = 4$ can be used. For lower SNR cases, a value of $\sigma = 1$ was required to reliably track the vortex. The cost weight factor (γ) can be scaled from zero to one based on the complexity of the vortex path. For a complex vortex path, e.g., hovering IGE, lower values of γ should be used compared to the case with a smooth vortex path. The path coordinates postfilter size and subsampling factor, p and s, respectively, can also be used to alter the path choice of the algorithm. By decreasing the path coordinate parameters, more complex paths can be traced but with an increased sensitivity to background noise. The window size factor in pixels, w, is only of importance when the

user is selecting the start and end points of the path. The window size is used to find the lowest cost pixel within the defined window and snaps the cursor to corresponding pixel. For the test case images selected, the values listed in Table 1 were found to produce the best results with the least amount of user interaction unless otherwise specified. Ultimately, the value of the parameters the researcher uses depends on the required accuracy, the SNR of the vortex signature to background, the complexity of the vortex path and the amount of desired user interaction.

Table 1: NeuronJ Parameters, Modified from Ref. 6

Parameter	Value	Description
σ	1	Gaussian smoothing Scale
γ	0.5	Cost components weight factor
w	9	Snapping window size, px
p	5	Path coordinates post-filter size, px
s	5	Path coordinates sub-sampling size, px

RESULTS

The neurite tracing algorithm was compared to traditional vortex tracing methods to quantify its advantage in maintaining or increasing the accuracy of the vortex path while reducing the post-processing time.

Case 1: BOS Image

For the first case, a BOS image was chosen that presented many of the challenges of tracing a tip vortex outlined in the introduction: low SNR, background blemishes, background seams and intersecting vortices. The Case 1 image is a BOS image from Ref. 2 and is shown in Fig. 2a. The first derivate with respect to the *y* direction of Fig. 2a was taken to create the image shown in Fig. 2b. The line profile plots for the original BOS image and first derivatives are shown in Figs. 3a and 3b, respectively, for lines defined as 1 and 2 in the figures.

First, looking at the relative pixel shift in Fig. 3a, the relative strength of the vortices can be determined. Line 1 is a slice of vortex 3, which is easily distinguishable by the double peak in intensity. The signature is approximately 10 pixels wide from y pixel 6 to pixel 16 on the vertical axis and has a peak to peak intensity of 140 counts. Line 2 is a slice of vortex 4 and is more difficult to distinguish from the background; however, by closer inspection, the vortex signature can be defined from approximately pixel 4 to pixel 12 on the vertical axis and a peak to peak intensity of 35 counts. The profile line plots in Fig. 3b are a representation of the signature that the neurite algorithm is seeking to trace. The signature is the same as that of a shadowgraph image in which a single peak of low intensity (dark line) exists on a high intensity noisy background.

The tracings obtained using the neurite tracing algorithm with the parameters found in Table. 1 are shown overlaid on original image in Fig. 2c. In all of the cases, the vortex paths

were obtained by clicking at the start and end of the vortex path. The local snapping feature eliminates the need for the researcher to precisely define the start/end points of the vortex given the vortex core is within the defined window size. The path between the start and end points was populated automatically by the neurite tracer.

To form comparisons to current methods, the same vorticies were traced using manual and cross-correlation template methods. For the fully manual tracing, a total of four researchers were asked to trace each vortex using a total 25 points per vortex. For the cross-correlation template method, a point along the vortex was selected and the automated path was generated using the algorithm described in the introduction and in detail in Ref. 5. The comparison of the vortex paths using all three methods is shown in Fig. 4. The vortex numbers are defined by labels on Fig. 2c. The solid lines represent the neurite algorithm path, the closed symbols represent manual user selection and the open symbols represent the cross-correlation template method. In general, the manual selection method compares well with the neurite tracing method for all five vorticies. The results from all three tracing methods were compared for vorticies 1, 2 and 4 because they are a subset of the difficulties in tracing a rotor tip vortex. Each of these three vortices were analyzed in more detail in order of tracing difficulty.

Vortex 3 is an example of a vortex with high SNR without background discontinuities. Vortex 3 represents the easiest vortex to trace because many of the difficulties are not present on the path of the vortex. If one ignores the intersection with vortex two, all three tracing methods produce nearly the same vortex path with small differences of 0.25-1.00 pixel between the paths.

Vortex 1 is an example of a vortex with high SNR but with several background discontinuities. For manual selection, the background discontinuities are easily ignored by the researcher that selects points on either side of a discontinuity. The cross-correlation template method is unable to ignore the background discontinuities and cannot accurately track the vortex after a discontinuity. The inability to track the vortex after a discontinuity is a result of the template being updated with the pixel intensity information from the discontinuity. It is feasible that large discontinuities could be masked from the tracing algorithm prior to the tracing; however, distributed background noise could not be masked. An example of this type of problem is shown in Case 2 where the SNR is very low.

Vortex 4 is an example of a vortex with lower SNR and several background discontinuities. The manual selection method results in higher path scatter than vortices with high SNR. The average path of the manual method is close to that of the neurite trace. The cross-correlation template method cannot accurately trace the vortex due the background discontinuities and the low SNR.

Since the cross-correlation template method has obvious shortcomings in tracking the vortex path, only the manual and

neurite tracing paths were analyzed for their quantitative differences. The pixel difference between the neurite path and the all of the manual paths were calculated and are shown in Table 2. For vorticies 1, 2 and 3, the mean pixel difference and standard deviation was less than one pixel and the maximum pixel difference ranged from 1.9 to 7.1. As shown in the profile line plots in Fig. 3a, the vortex width is approximately ten pixels for this image. Therefore, the pixel shift is within the bounds of the detected vortex. For vorticies 4 and 5, many of the researchers reported that the vortex was very difficult to distinguish from the background. Despite the difficulties, the mean pixel shift ranged from 1.7 to 4.1 for vorticies 4 and 5, respectively. The maximum were 8.6 and 7.6 with standard deviations of 1.63 and 1.33. In most cases, the researchers did not identify the full lateral extent of the vortex.

Table 2: Pixel Differences between Manual and Neurite Tracing Vortex Paths

Vortex Number	Mean	Max	Standard Deviation
Vortex 1	0.6	1.9	0.47
Vortex 2	0.8	2.7	0.76
Vortex 3	0.9	7.1	0.95
Vortex 4	1.7	8.6	1.63
Vortex 5	4.1	7.6	1.33

By using the neurite tracing method for this case, a researcher's workload could be reduced by a factor of 12.5. This time savings assumes an equal amount of time per mouse click with two mouse clicks per neurite tracing and 25 mouse clicks per manual tracing. Depending on the level of detail required in the manual tracing and the amount of user interaction for the neurite tracing, the actual time savings may vary from case to case.

Case 2: BOS Image Pair

For Case 2, a pair of BOS images from Ref. 2 were evaluated because they were considered some of the highest noise images and required fully manual tracings during the original post-processing. In addition to the low SNR, the images had several background discontinuities near the vortex paths. The processed BOS pixel shifts for the two images are shown in Fig. 5a and 6a. The two neurite traced vortices represented by the solid blue lines in Figs. 5c and 6c were determined using two mouse clicks per vortex (one at the start/end). The red open circles represent an attempt to use the cross-correlation template method. Obviously the method has profound difficulties in tracking the vortex in these types of images, which was the motivation for this work.

Case 3: Shadowgraph Image Pair Example

The neurite tracing method is also capable of tracing vortices obtained using shadowgraph imaging. In Case 3, a set of shadowgraph image pairs were traced using the neurite tracer then located in 3-D space using photogrammetry. In ImgA,

shown in Fig. 7, two tip vortices were traced using the neurite tracer with two mouse clicks per vortex. In ImgB, shown in Fig. 8, only one vortex was visible in the field of view and was traced using the neurite tracer. In ImgB, there was a significant amount of noise in the image due to imperfections in the tunnel windows that the cameras looked through rather than the background. Despite the noise, the neurite tracer was able to reliably trace the vortex using two mouse clicks.

After determining the pixel locations of the vortex trailing from the current blade from each image, the 3D position of the vortex could be determined using photogrammetry. Since the vortex from the previous blade is only visible in one of the image pairs, it could not be located in 3-D space. The photogrammetry setup and data processing is not the focus of this paper, but the process that is outlined in Section V. of Ref. 2 was used with the exception of the manual tracing in step three, which was replaced by the neurite tracing. As shown in Fig. 9, the neurite tracings from Figs. 7b and 8b can be converted to a 3D representation of the tip vortex location. The tip vortex is represented by the red circles in relation to the rotor blades and fuselage.

This case was also selected to show how a series of similar images could be batch processed using the neurite tracer. It is common practice to take at least 100 images of the same rotor azimuth. In an ideal case, the images are averaged and the vortex only needs to be traced for one averaged image. If the vortex location in each individual frame needs to be determined, the local window snapping option can be use to automate the image set. For Case 3 ImgB, a region of interest (ROI) was defined by the red box in Fig. 8a. Within this ROI, start and end points were defined with a local window size of 9x9 pixels. The neurite tracer was run using the same start/end points for a series of ten images. The resulting traces for three images, for clarity, are shown in Fig. 10. The slight variations in the vortex path due to flow unsteadiness are captured by the neurite tracer. The automated tracing can be extended to a case where the vortex paths have greater variation from image to image by using a modified window size. Using the ROI defined in Fig. 7a by the red rectangle, the tracing can be automated for varying rotor azimuths. First, a start pixel location of $x = 0, y = 250$ and end pixel location of $x = 1150, y = 480$ was selected with a window size of $w = 3x100$. By using a vertical window, the vertical changes in the vortex track can easily be accounted for as the azimuth delay is varied. The results are shown in Fig. 11 where the changes in the vortex path are automatically traced for changes in rotor azimuth.

Case 4: Shadowgraph Complex Path Example

The final example is of a case with a complex tip vortex path. A shadowgraph image of tip vortices from a rotor hovering IGE was used as shown in Fig. 12a. A hovering rotor IGE creates a very complex flow field in which the tip vortex path is highly 3-D and aperiodic. The resulting neurite tracing of the image is shown in Fig. 12b. For this case, the cost components weight factor was set equal to $\gamma = 0.2$ to account for

the complex paths of the vortices. By reducing the cost components weight factor, the amount of user interaction could be reduced but not eliminated. The points identified on the figure by the red and white crosses represent the approximate mouse click locations required to generated the traces in blue. For vorticies 1, 2 and 3, only two mouse clicks were required. For the remaining vortices, which had more complex paths, between three and seven mouse clicks per vortex were required to accurately trace the vortices. Even with the increased user interaction for this case, the total workload of the researcher is significantly reduced compared to a fully manual tracing that would require on the order of 25 clicks per vortex for a total of 175 clicks compared to that of 23 for the neurite tracing.

CONCLUDING REMARKS

A neurite tracing algorithm originally developed for semi-automatic tracing of the human brain and other medical images was evaluated for the use of tracing rotor tip vortex images obtained via density gradient imaging techniques. Several sample images were used to form four case studies that included both BOS and shadowgraph images. In general, the neurite tracing algorithm provided a significant reduction in the post-processing time without comprising the accuracy of the tip vortex location. The vortex paths generated with the neurite tracing algorithm were benchmarked against the current standard of fully manual tracing and an alternative method using a cross-correlation template method. The compromising show that the fully manual and neurite tracing methods had increased accuracy over that of the cross-correlation template method, which is highly susceptible to background noise and discontinuities. The neurite tracing method can reduce the number of mouse clicks and thus, workload by a factor of 10 to 15 depending on the level of detail required in the path tracing. Finally, the neurite tracing method can be setup in a batch processing mode to post-process large volumes of data.

ACKNOWLEDGMENTS

REFERENCES

[1]Leishman, J. G., *Principles of Helicopter Aerodynamics*, Cambridge University Press, New York, NY, 2000, pp. 568–572.

[2]Schairer, E., Kushner, L., Heineck, J., and Walker, L., "Retroreflective Background Oriented Schliern Tip Vortex Visualization and Mapping for UH-60 Airloads," *American Helicopter Society 69th Annual Forum Proceedings*, 2013.

[3]Bauknecht, A., Merz, C., Raffel, M., Landolt, A., and Meier, A., "Blade Tip Vortex Detection in Maneuvering Flight using the Background Oriented Schlieren (BOS) Technique," *American Helicopter Society 69th Annual Forum Proceedings*, 2013.

[4]Bauknecht, A., Ewers, B., Wolf, C., Raffel, M., and Leopold, F., "Three-dimensional reconstruction of blade tip vortices of a BO 105 using a multi-camera BOS system," *American Helicopter Society 70th Annual Forum Proceedings*, 2014.

[5]Meyn, L. and Bennett, M., "Application of a Two Camera Video Imaging System to Three-Dimensional Vortex Tracking in the 80- by 120-Foot Wind Tunnel," *AIAA Applied Aerodynamics Conference*, 1993.

[6]Meijering, E., Jacob, M., Sarria, J., Steiner, P., Hirling, H., and Unser, M., "Design and Validation of a Tool for Neurite Tracing and Analysis in Fluorescence Microscopy Images," 2004.

[7]Rasband, W., "ImageJ," *U. S. National Institutes of Health, Bethesda, MD, http://imagej.nih.gov/ij/*, 1997-2015.

(a) Case 1- Processed BOS Image, Δy, Ref. 2

(a) Fluorescence Microscopy Image of Human Brain from Ref. 6
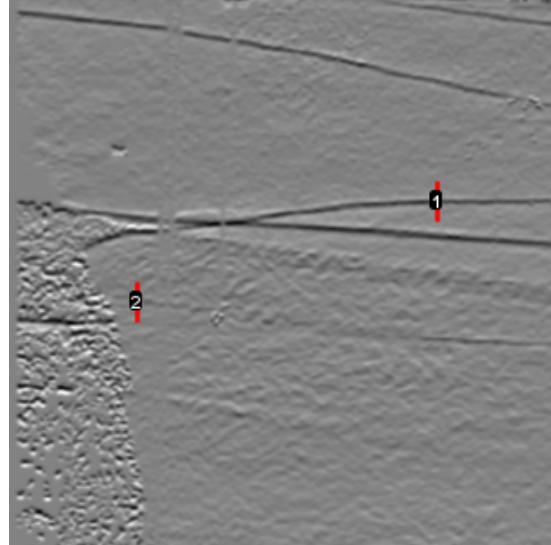
(b) Case 1- First Derivative of Processed BOS Image, $\frac{\partial \Delta y}{\partial y}$

(b) Sample Shadowgraph Image, Hovering IGE

Fig. 1: Comparison of Image Types
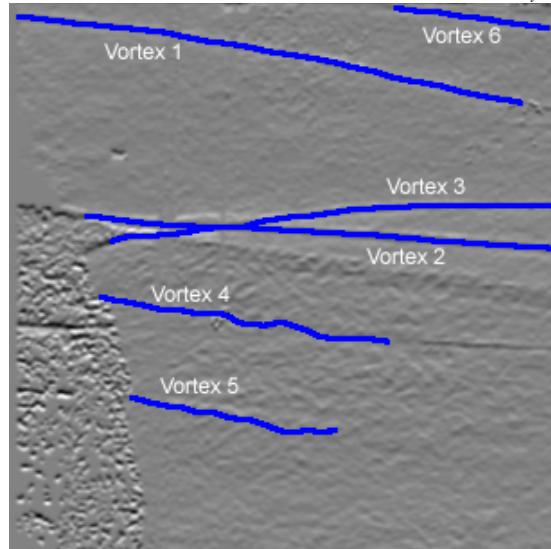
(c) Case 1- Neurite Tracing of First Derivative of BOS Image

Fig. 2: Case 1
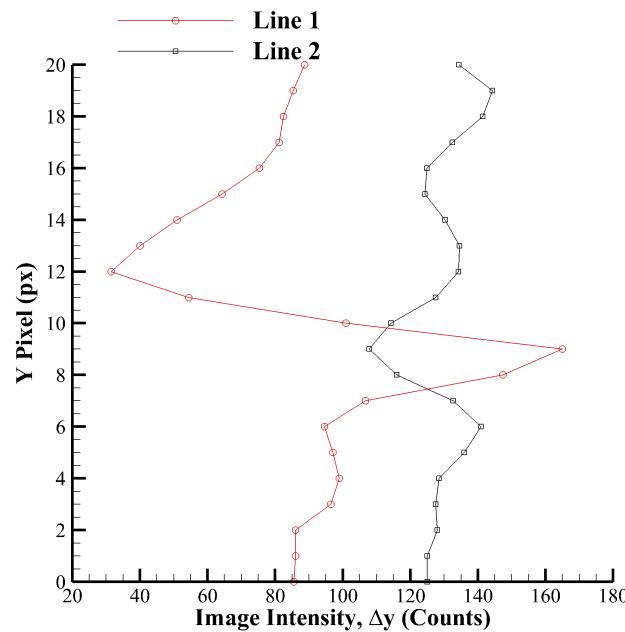
(a) Pixel Shift Line Intensity
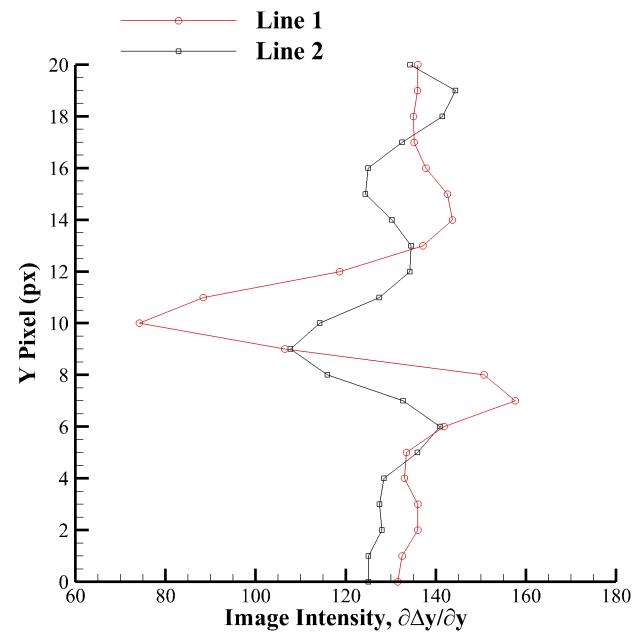
(b) First Derivative of Line Intensity

Fig. 3: Profile Line Plots from Fig. 2b
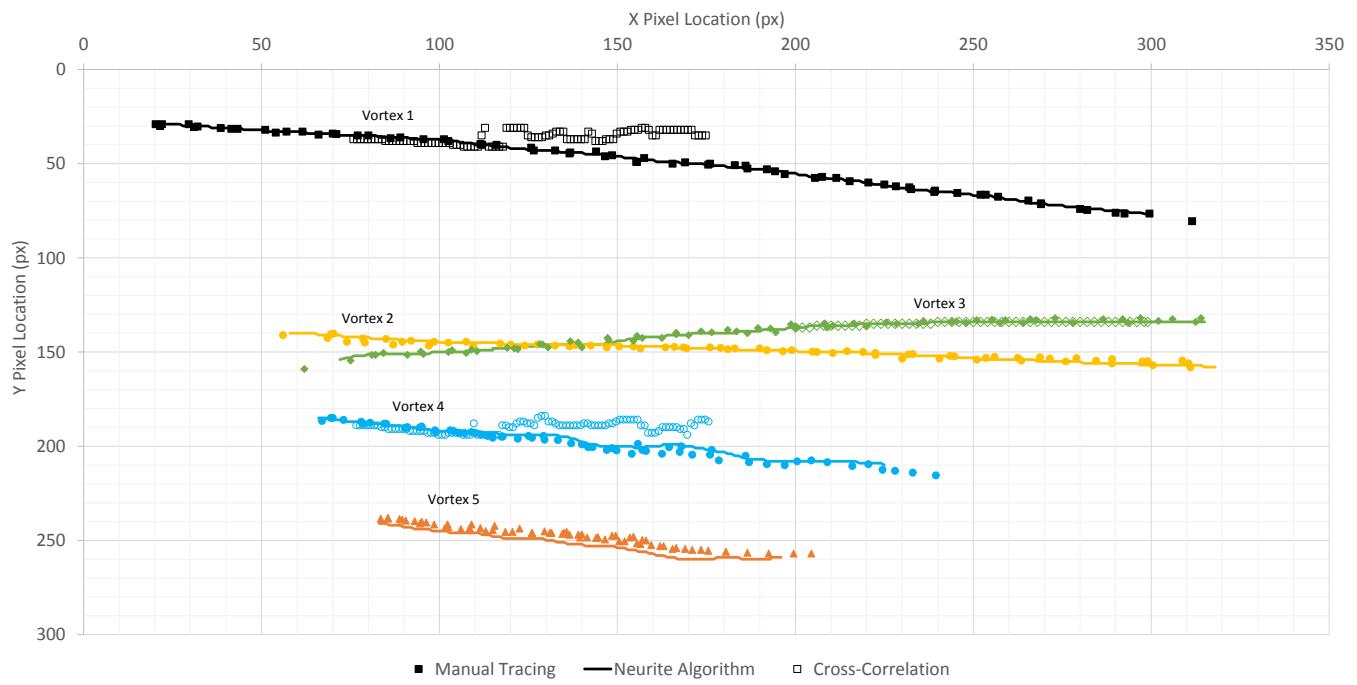
Fig. 4: Case 1- Comparison of Tracing Techniques
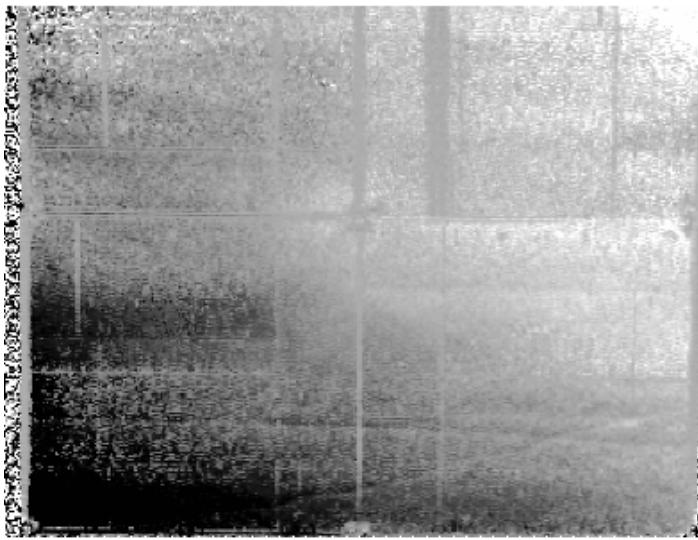
(a) Case 2- ImgB Processed BOS Image, Δy, Ref. 2

(a) Case 2- ImgA Processed BOS Image, Δy, Ref. 2

(b) Case 2- ImgB First Derivative of Processed BOS Image, $\frac{\partial \Delta y}{\partial y}$
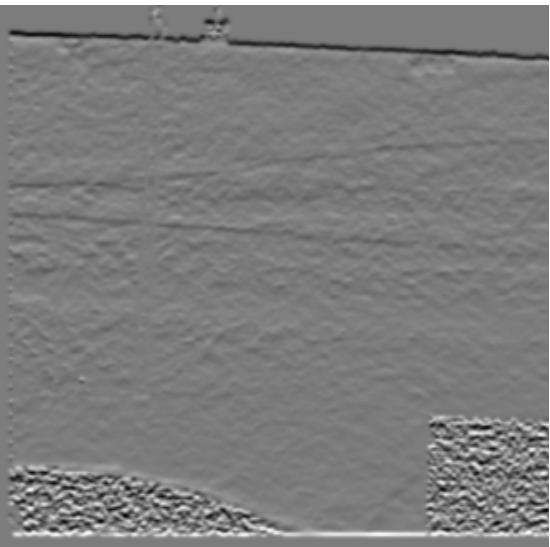
(b) Case 2- ImgA First Derivative of Processed BOS Image, $\frac{\partial \Delta y}{\partial y}$

(c) Case 2- ImgB Neurite Tracing
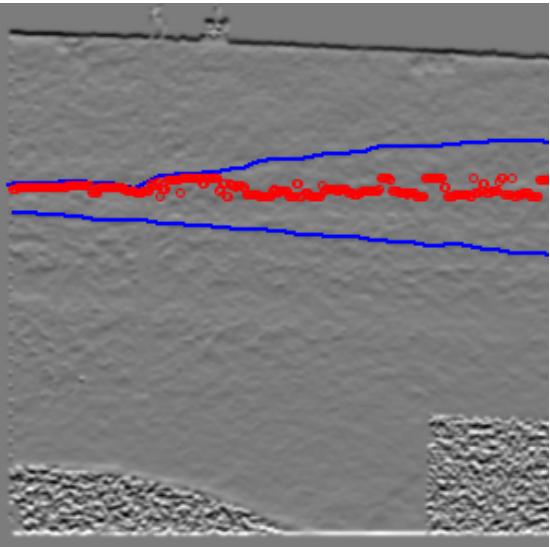
(c) Case 2- ImgA Neurite Tracing

Fig. 5: Case 2- ImgB

Fig. 6: Case 2- ImgA
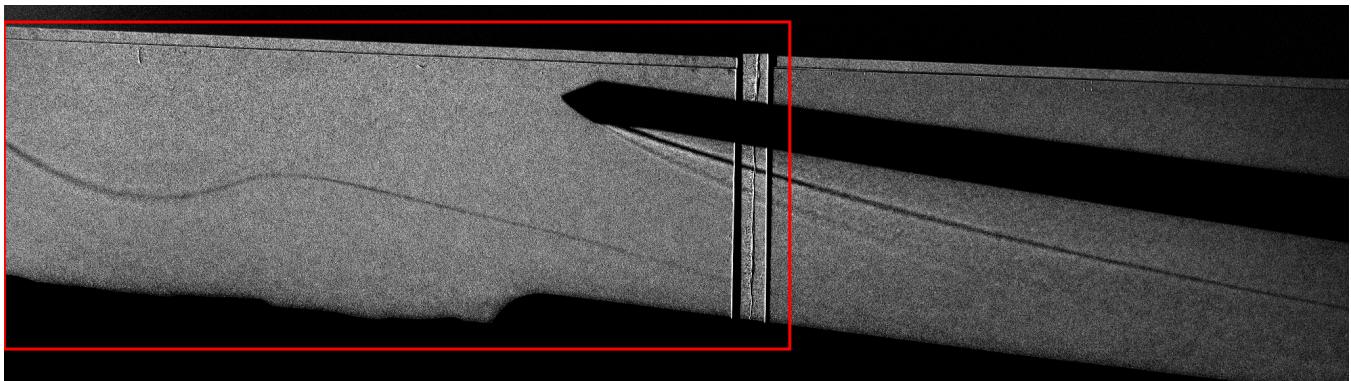
(a) Case 3- Shadowgraph ImgA Background Subtracted
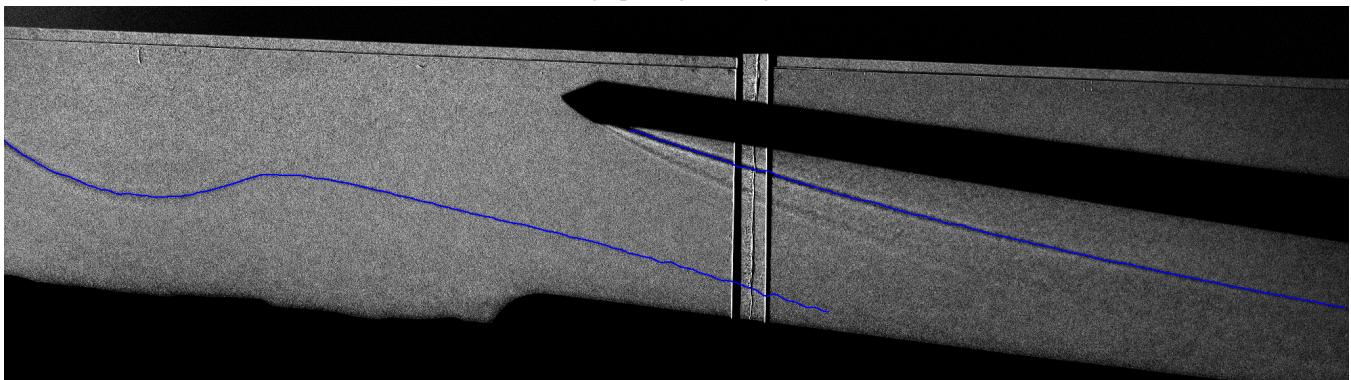
(b) Case 3- Shadowgraph ImgA Neurite Tracing

Fig. 7: Case 3- ImgA
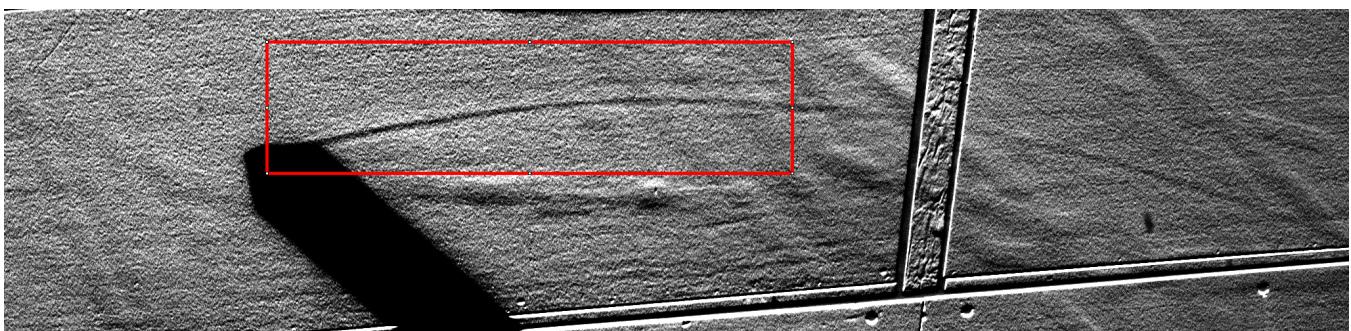
(a) Case 3- Shadowgraph ImgB Background Subtracted
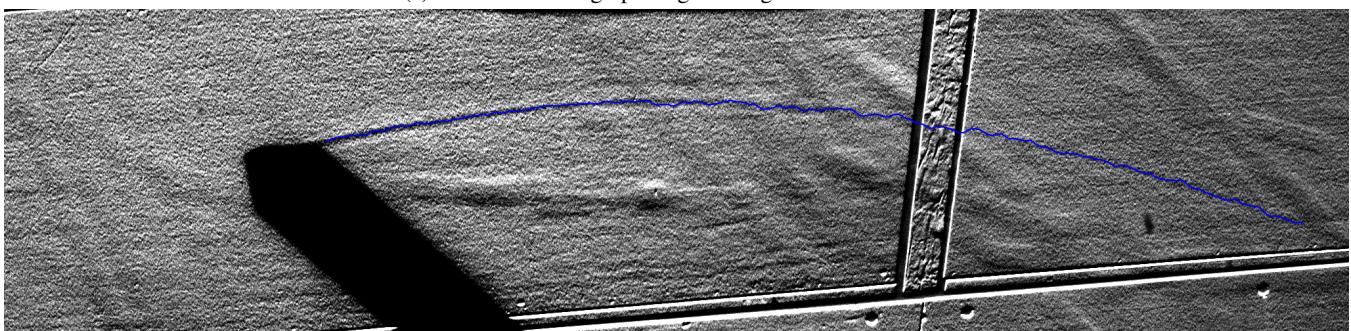
(b) Case 3- Shadowgraph ImgB Neurite Tracing

Fig. 8: Case 3- ImgB
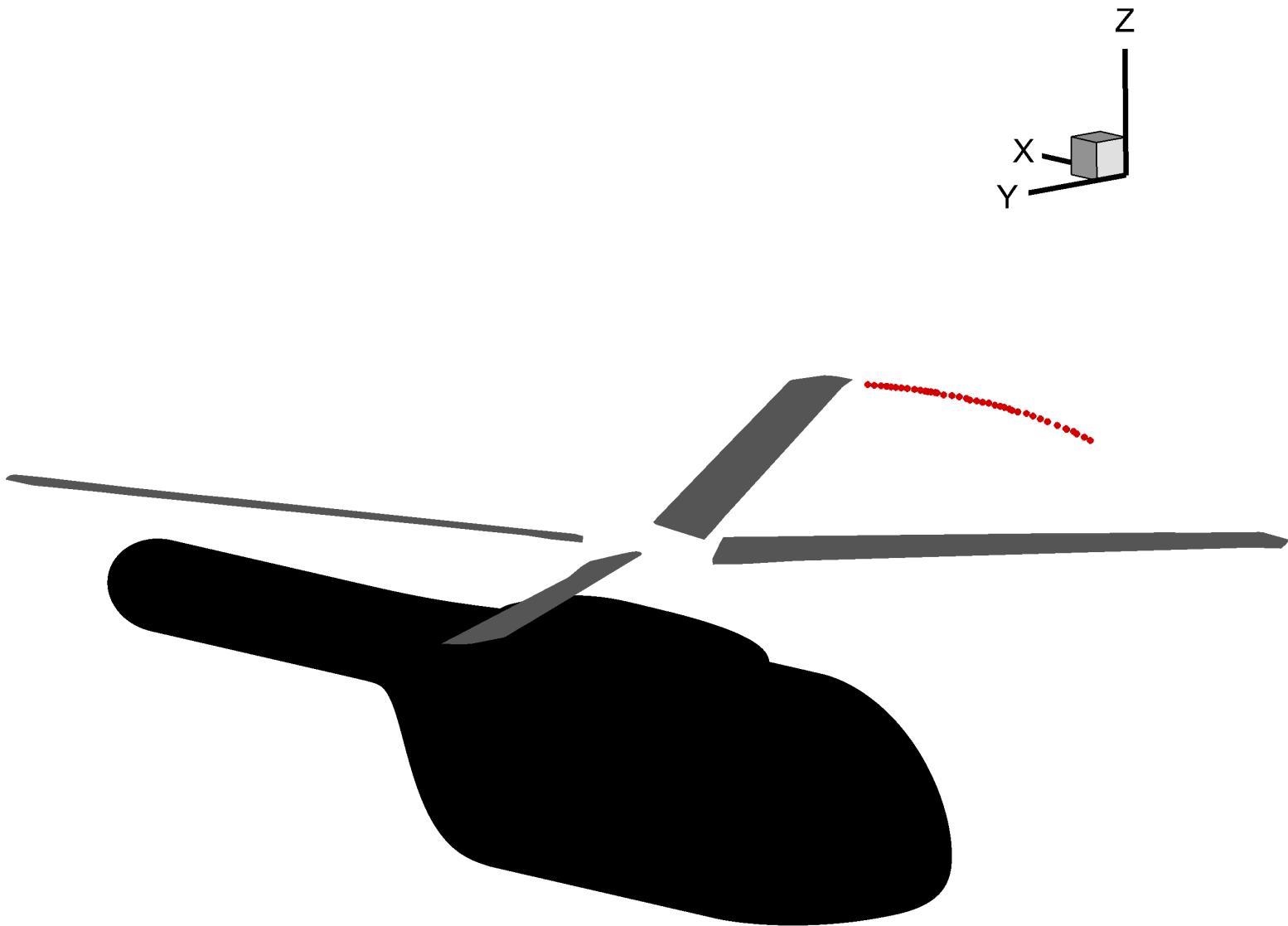
Fig. 9: Sample Vortex Location in 3-D Space from Case 3
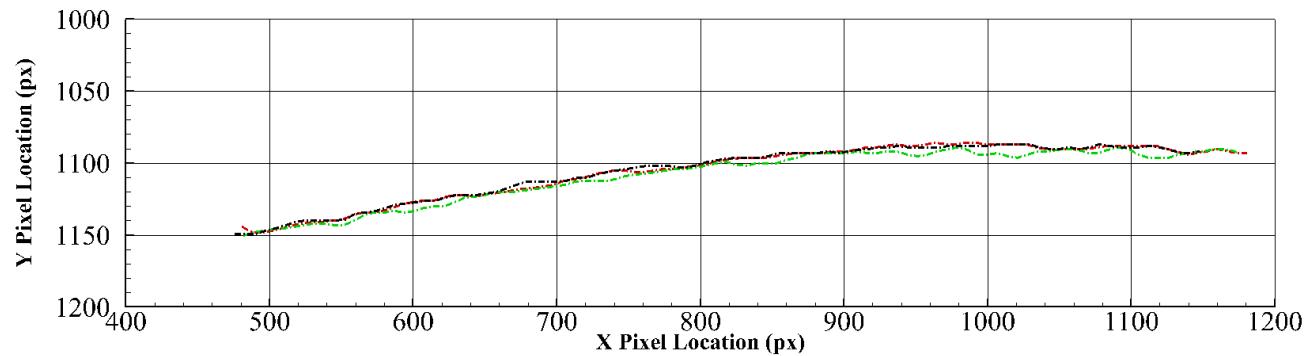
Fig. 10: Automated Tracing for Image to Image Variations, from ROI in Fig. 8a
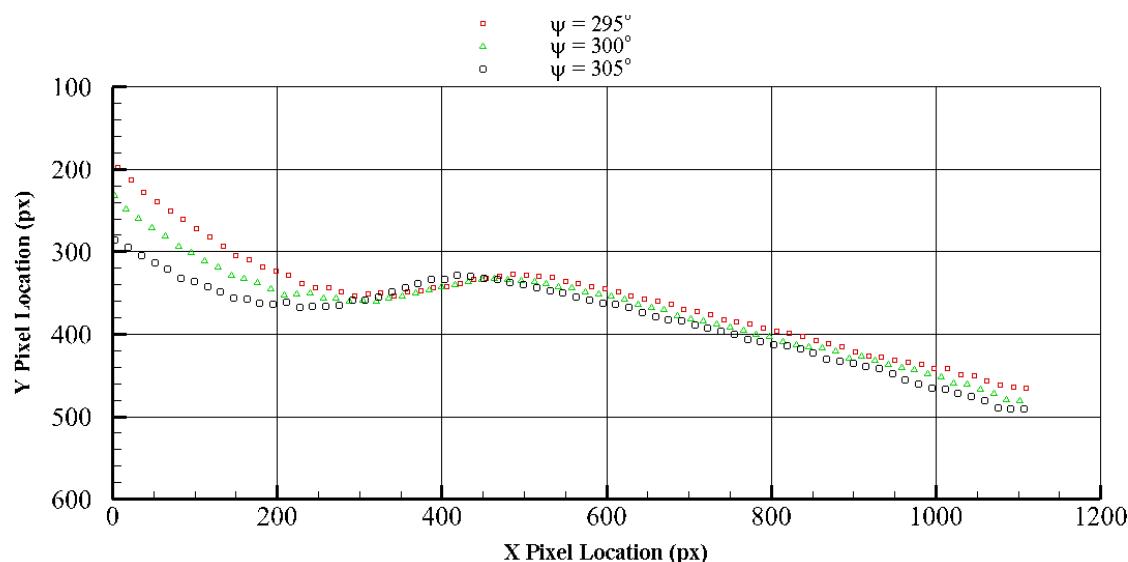

Fig. 11: Automated Tracing for Changing Rotor Azimuths, from ROI in Fig. 7a
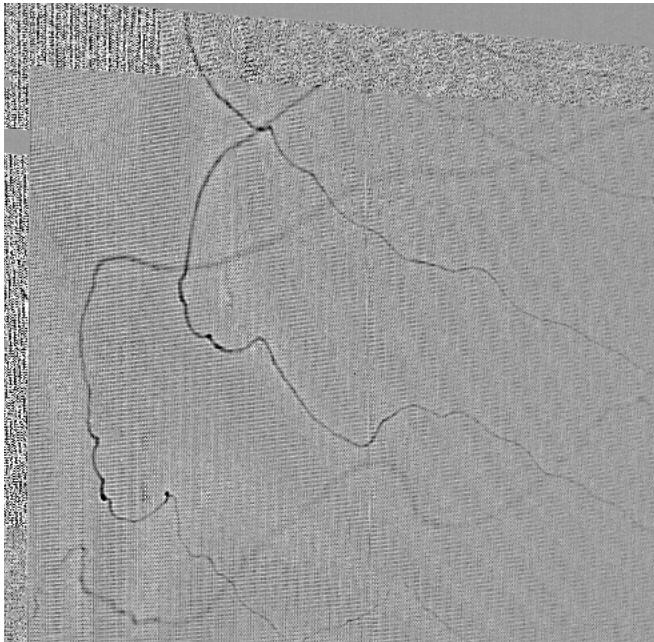
(a) Shadowgraph Image
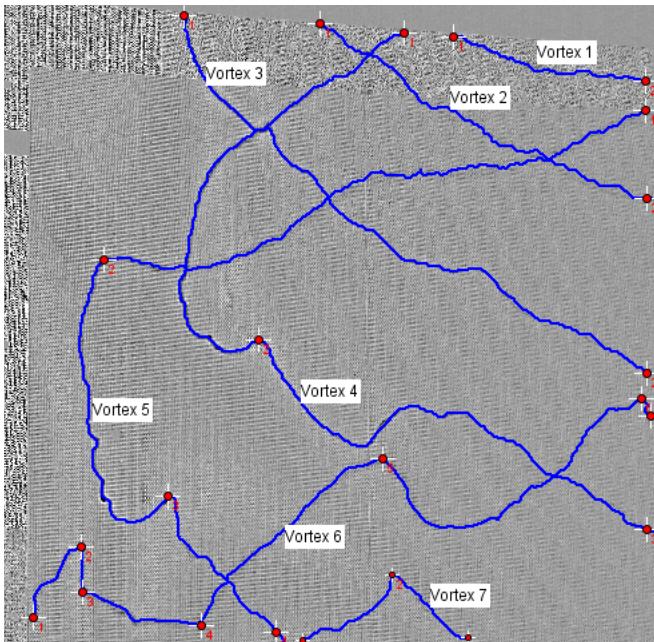
(b) Neurite Tracing of Shadowgraph Image

Fig. 12: Case 4- Shadowgraph Complex Path Example from a rotor Hovering IGE